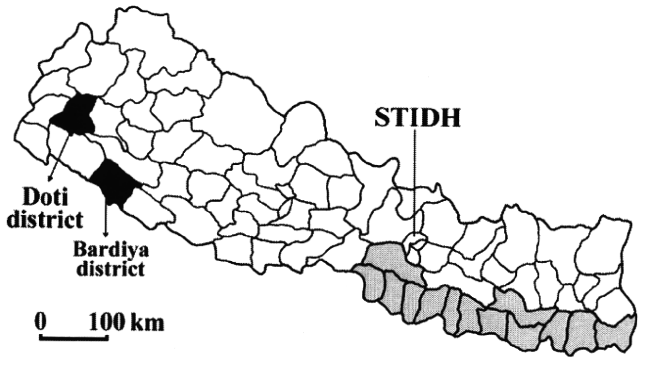

FIGURE 1. District maps of Nepal. Districts endemic for leishmaniasis are indicated in grey. The VL patient reported resides in the hilly district Doti (black). The Bardiya district, where a suspected miltefosine-resistant VL case was previously reported, is indicated (black). STIDH indicates the Sukraraj Tropical and Infectious Disease Hospital.

DISCUSSION

This is the first report of VL from the non-endemic far western hilly region of Nepal. Nepal is geographically divided into three areas: the Mountain, Hills, and Terai regions. VL transmission generally occurs in plain Terai region, with an altitude of a maximum of 305 m. However, cases have been increasingly reported from hilly regions of India and the eastern part of Nepal in the recent years.[2,5] VL has been considered to be a disease of low altitude and is usually found below the altitude of 600 m (2,000 ft) above sea level.[6] In the present report, however, VL is found in the hilly, far western region at an altitude of 1,113 m (3,654 feet) above sea level. VL cases from hilly regions above the altitude of 1,000 m have been reported in India,[7,8] which could be because of the improved monitor system, changes in seasonal climate over the past years, and potential changes of geographical distribution of the vectors. Previously, we have reported a VL case from midwestern region of Nepal.[9] However, it was unclear if this patient was infected with VL in this region because of the history of traveling to India. In this study, however, the patient had no history of traveling to India or VL endemic regions of Nepal, suggesting that VL was expanding into newer areas. The transmission of the *Leishmania donovani* needs a vector sandfly and potentially, reservoir animals; however, this information in the hilly region of Nepal, including the Doti district, is not available. Active VL and entomological surveillance are warranted in the far western region of Nepal to confirm this point. The patient reported in this study showed VL symptoms within 1 year after the complete standard VL treatment; however, treatment with the same drug, Amphotericin B, was able to cure this patient, suggesting that the relapse was likely not caused by the drug resistance of the parasites. The precise reason of the relapse is unclear and not the major point in this study. VL is a major health problem in Nepal and is endemic in 13 districts of the eastern and central Terai region. According to annual health report of the Department of Health Services in Nepal, VL incidence has shown to be 2.67 per 10,000 people at risk in 2006–2007.[2] The VL elimination program aims at reducing incidence to 1 per 10,000 at risk by the year 2015. An increasing trend of sporadic VL cases from other parts (non-endemic regions) of the country like Doti could challenge the aim of the VL elimination program. In addition, findings of drug resistance reports from newer areas could be another obstacle in reducing the morbidity and mortality rate in the long term in Nepal. Thus, policy makers should give a high priority in expanding active VL surveillance network in the newly parasite-detected areas to achieve the realistic goal by the year 2015.

Received May 21, 2010. Accepted for publication September 5, 2010.

Acknowledgments: We gratefully thank to the director and staff of the Sukraraj Tropical and Infectious Diseases Hospital for providing care to the patients and facility. We would also like to thank Mr. Kiran Pandey at the Everest International Clinic and Research Center, Kathmandu, Nepal, for his technical support. Assessment and treatment of patients was carried out in accordance with standard clinical procedures at the Sukraraj Tropical and Infectious Diseases Hospital, Kathmandu, Nepal. Informed consent was obtained from the patients for their assessment, treatment, and publication of the case report. B.D.P. performed the clinical evaluation and management of the cases; B.D.P. and S.B.P. drafted the manuscript, and O.K., K.P., and K.H. revised the paper. All authors read and approved the final manuscript.

Financial support: This study was supported in part by Grants-in-Aid from Ministry of Education, Culture, Sports, Science and Technology (MEXT), the Global Center of Excellence (COE) Program at Nagasaki University (to O.K. and K.H.), and the National Bio-Resource Project (NBRP) of MEXT, Japan (to K.H.).

Authors' addresses: Basu Dev Pandey and Sher Bahadur Pun, Sukraraj Tropical and Infectious Diseases Hospital and Everest International Clinic and Research Center, Kathmandu, Nepal, E-mails: basupandey@wlink.com.np and drsherbdr@yahoo.com. Osamu Kaneko, Department of Protozoology, Institute of Tropical Medicine (NEKKEN) and the Global Center of Excellence Program, Nagasaki University, Nagasaki, Japan, E-mail: okaneko@nagasaki-u.ac.jp. Kishor Pandey, Everest International Clinic and Research Center, Kathmandu, Nepal, E-mail: pandey_kishor@hotmail.com. Kenji Hirayama, Department of Immunogenetics, Institute of Tropical Medicine (NEKKEN) and the Global Center of Excellence Program, Nagasaki University, Nagasaki, Japan, E-mail: hiraken@nagasaki-u.ac.jp.

REFERENCES

1. Pandey K, Pant S, Kanbara H, Shuaibu MN, Mallik AK, Pandey BD, Kaneko O, Yanagi T, 2008. Molecular detection of *Leishmania* parasites from whole bodies of sandflies collected in Nepal. *Parasitol Res 108:* 293–297.
2. World Health Organization, 2005. Regional technical advisory group on kala-azar elimination. Proceedings of the 1st Meeting, December 20–23, 2004; New Delhi, India.
3. Department of Health Sciences, 2007. *Annual Report on Nepal.* Kathmandu, Nepal, 145–148.
4. Rijal S, Chappuis F, Singh R, Bovier PA, Acharya P, Karki BM, Das ML, Desjues P, Loutan L, Koirala S, 2003. Treatment of visceral leishmaniasis in south-eastern Nepal: decreasing efficacy of sodium stiboglucanate and need for the policy to limit further decline. *Trans R Soc Trop Med Hyg 97:* 350–354.
5. Joshi S, Bajracharya BL, Baral MR, 2006. Kala-azar (visceral leishmaniasis) from Khotang. *Kathmandu Univ Med J 4:* 232–234.
6. Park K, 2007. Leishmaniasis. Park K, ed. *Park's Text Book of Preventive and Social Medicine*, 6th ed. Jabalpur, India: Banarsidas Bhanot, 256–258.
7. Verma SK, Ahmed S, Shirazi N, Kusum A, Kaushik RM, Barthwal SP, 2007. Sodium stibogluconate-sensitive visceral leishmaniasis in the non-endemic hilly region of Uttarkhand, India. *Trans R Soc Trop Med Hyg 101:* 730–732.
8. Mahajan SK, Machhan P, Kanga A, Thakur S, Sharma A, Prasher BS, Pal LS, 2004. Kala-azar at high altitude. *J Commun Dis 36:* 117–120.
9. Pandey BD, Pandey K, Kaneko O, Yanagi T, Hirayama K, 2009. Relapse of visceral leishmaniasis after miltefosine treatment in a Nepalese patient. *Am J Trop Med Hyg 80:* 580–582.

Parasitol Res (2010) 107:727–730
DOI 10.1007/s00436-010-1920-0

SHORT COMMUNICATION

Diagnosis of visceral leishmaniasis by polymerase chain reaction of DNA extracted from Giemsa's solution-stained slides

Kishor Pandey · Basu Dev Pandey · Arun Kumar Mallik · Osamu Kaneko · Haruki Uemura · Hiroji Kanbara · Tetsuo Yanagi · Kenji Hirayama

Received: 30 April 2010 / Accepted: 7 May 2010 / Published online: 25 May 2010

Abstract Visceral leishmaniasis (VL) is caused by the protozoan parasite *Leishmania donovani* and is a potentially fatal disease in endemic areas of the world. Nepal is an endemic area in which VL causes major public health problems in the lowland areas of the southeast regions. The aim of the present study was to evaluate the sensitivity of polymerase chain reaction (PCR) amplification for the detection of *Leishmania* DNA from Giemsa's solution-stained bone marrow slides. Bone marrow samples were aspirated from a total of 115 VL suspected patients and used to prepare smears on glass slides and for the initiation of in vitro culture. Bone marrow slides were used for microscopic observation, DNA extraction, and subsequent PCR amplification. PCR analysis showed that all the positive samples were of *Leishmania* parasites. The PCR assay also showed a higher sensitivity (69%) than microscopic examination (57%) and culture (21%). In addition, PCR was able to detect VL in 12% of samples which were negative by microscopy. PCR of DNA extracted from Giemsa's solution-stained bone marrow slides is a suitable tool for confirming diagnosis in patients with VL and may also be useful in the diagnosis of difficult cases. Bone marrow smears are easily stored and can be easily sent to research centers where PCR is available. This makes PCR a good option for diagnosis in the field.

K. Pandey (✉) · K. Hirayama
Department of Immunogenetics, Institute of Tropical Medicine (NEKKEN) and the Global COE Program, Nagasaki University, 1-12-4 Sakamoto,
Nagasaki 852-8523, Japan
e-mail: pandey_kishor@hotmail.com

K. Hirayama
e-mail: hiraken@nagasaki-u.ac.jp

B. D. Pandey
Sukraraj Tropical and Infectious Diseases Hospital,
Kathmandu, Nepal
e-mail: basupandey@wlink.com.np

A. K. Mallik
Janakpur Zonal Hospital,
Janakpur, Nepal
e-mail: ak_mallik@yahoo.com

O. Kaneko · H. Uemura · H. Kanbara
Department of Protozoology, Institute of Tropical Medicine (NEKKEN) and the Global COE Program, Nagasaki University, 1-12-4 Sakamoto,
Nagasaki 852-8523, Japan

O. Kaneko
e-mail: okaneko@nagasaki-u.ac.jp

H. Uemura
e-mail: uemura@nagasaki.net-u.ac.jp

T. Yanagi
Animal Research Center for Tropical Infections,
Institute of Tropical Medicine, Nagasaki University,
1-12-4 Sakamoto,
Nagasaki 852-8523, Japan
e-mail: tyanagi@tm.nagasaki-u.ac.jp

Introduction

Visceral leishmaniasis (VL) is a parasitic disease caused by the protozoan parasite *Leishmania donovani* and is transmitted by sand fly vectors. VL has been reported from 51 countries around the world and has an annual incidence of 500,000 cases. VL is responsible for about 59,000 deaths per year and 2.4 million disability-adjusted life years are lost worldwide. India, Nepal, and Bangladesh account for 300,000 cases annually, and thus account for 60% of the total global burden of this disease. In Nepal,

VL causes major public health problems as well as mortality in the lowland areas of the southeast regions which border Bihar Indian state, a known VL endemic area. Early treatment is a major pillar of the current VL elimination program, which has been launched by the governments of India (Aransay et al. 2000), Nepal, and Bangladesh (Sundar et al. 2008; Al-Jawabreh et al. 2003).

The gold standard method for VL diagnosis is microscopical examination of *L. donovani* bodies in bone marrow aspirates. Such detection of *Leishmania* parasites in a clinical sample is necessary to confirm a suspected case of VL. The most common method for VL diagnosis is direct detection of parasites, either by microscopical examination or in vitro cultivation, for which sensitivity is low (Herwaldt 1999). Other methods for diagnosis of VL, such as parasitological or serological tests, are difficult even in well-equipped hospitals (Sundar 2003; da Silva 2005). As an alternative at the district level, serological tests (direct agglutination test or rK39 immunochromatographic test) were used. The minimum basis for starting treatment for VL is positivity for rK39 immunochromatographic test. The serodiagnosis is negative in the early acute stage of the disease and do not differentiate between active, past, or subclinical infection. It remains positive well beyond the time of cure, thus limiting their use for the diagnosis of relapses or reinfection (Chappuis et al. 2007). Thus, improved tools for the diagnosis of VL are needed. Molecular methods including polymerase chain reaction (PCR)-based techniques have proven to be highly sensitive and specific as they analyze parasite DNA and may be applied to a variety of clinically obtained samples (Marfurt et al. 2003; Bensoussan et al. 2006; Schallig and Oskam 2002; Reithinger and Dujardin 2007; Brustoloni et al. 2007) For clinical samples, Giemsa's solution-stained bone marrow smears on glass slides are potentially very valuable sources of DNA for PCR-based diagnosis. Firstly, PCR diagnosis using DNA extracted from Giemsa's solution-stained bone marrow slides is a suitable tool to confirm diagnosis in patients with VL and is useful in the diagnosis of difficult cases. Secondly, historical slides or archived materials may be assessed, thus allowing retrospective studies. Lastly, bone marrow smears can be easily stored and sent to research centers where PCR diagnosis can be readily achieved.

A number of PCR-based diagnoses from Giemsa's solution-stained samples on glass slides have been previously reported, including blood smears for *Plasmodium* spp. (Li et al. 1997), for cutaneous Leishmaniasis (Motazedian et al. 2002), and fecal smears containing *Cryptosporidium parvum* (Amar et al. 2001). However, PCR-based *Leishmania* diagnosis from bone marrow smears on glass slides have not been widely applied, although we have recently described the use of this strategy to confirm VL infection of a Nepali patient (Pandey et al. 2009) Thus, in the present study, we have investigated the sensitivity of PCR diagnosis from bone marrow samples obtained from clinically suspected VL patients in comparison with microscopy and parasite culture.

Material and methods

Sample collection

Bone marrow samples were collected from clinically suspected VL patients on the basis of clinical history (continuous fever for 2 weeks, headache, and splenomegaly) in Nepal during 2003–2005. Bone marrow was aspirated by sternal puncture and used for smear preparation and to initiate *Leishmania* culture. Bone marrow smears were fixed with methanol and stained with Giemsa's solution. More than 100 microscopic fields were observed in order to detect the parasite. The slides were kept at room temperature and brought to Japan for further analysis. Informed consent from each of the patients was obtained after an explanation of the uses of bone marrow aspirates. The research protocol was approved by the Ethical Committee of Nagasaki University.

DNA extraction

After shipping to Japan, all bone marrow smear samples were re-examined microscopically for *Leishmania* parasite infection. Then, Giemsa's solution-stained smears were wiped with fresh paper wipes (Kimwipe wipers S-200; Kimberly-Clark, Dallas, TX) to remove immersion oil, wetted with sterile phosphate-buffered saline, and scraped with a sterile scalpel. The DNA was extracted by using the DNeasy Blood and Tissue Kit (Qiagen, Valencia, CA) according to the manufacturer's instructions, yielding a final elution volume of 25 μl. Two different reference strains of *L. donovani*, Dd8 Indian strain (accession no. Y11401) and T4 Nepalese strain (accession no AB458390), were used as positive controls for PCR amplification.

PCR amplification

We selected the conserved region of minicircle kinetoplast DNA because its copy number is more than 10^4 per parasite, maximizing the possibility of detection (Akkafa et al. 2008; Smyth et al. 1992; Salotra et al. 2001). PCR analysis consisted of two steps, the details of which were given previously (Aransay et al. 2000; Pandey et al. 2008). Briefly, first-round PCR amplification was carried out in a total of 10 μl reaction mixture with primers LINR4 (5′-

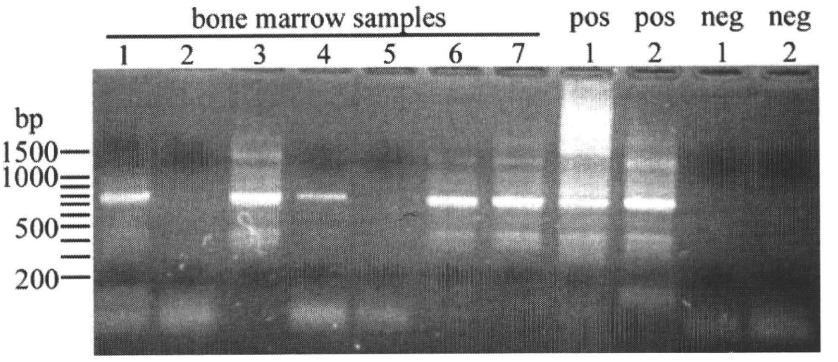

Fig. 1 PCR amplification of the *Leishmania* DNA obtained from Giemsa's solution-stained smears on glass slides. *Lanes 1–7* bone marrow samples, *pos1* and *pos2* DNA from cultured *Leishmania* parasite, *neg1* DNA from mouse bone marrow without *Leishmania* infection, *neg2* without DNA template. In this experiment, *sample numbers 1*, *3*, *4*, *6*, and *7* were judged to be positive for *Leishmania* infection

GGGGTTGGTGTAAAATAGGG-3′) and LIN17 (5′-TTTGAACGGGATTTCTG-3′) and 2 μl of DNA solution. The second-round seminested PCR was carried out in a 20-μl reaction mixture volume as for the first round by adding primer LIN19 (5′-CAGAACGCCCCTACCCG-3′) and 1 μl of the first PCR product. Two negative controls and two positive controls were set for each experiment. The first negative control was normal mouse bone marrow and the other was DNA-negative reaction mixture. Two positive controls contained DNA from cultured *L. donovani* parasites. Ten microliters of the PCR-amplified products were subjected to 2% agarose gel electrophoresis, stained with ethidium bromide, and visualized under UV light. A 100-bp DNA ladder was used as a marker.

Results and discussion

Microscopical examination, parasite culture, and PCR diagnosis using bone marrow smears were performed for 115 samples obtained from clinically suspected VL patients. Samples which produced a 720-bp band following PCR amplification and electrophoresis were judged to be positive for VL. Figure 1 shows an example of an agarose gel electrophoresis image. The positive controls produced the expected 720-bp band which was absent from the negative controls. Among 115 samples, *Leishmania* DNA was successfully detected in 79 samples. PCR diagnosis showed the highest sensitivity (79 positive/115 samples, 68.7%) compared to microscopical examination (65/115, 56.5%) and parasite culture (20/115, 21%; Table 1). All samples positive by microscopic examination or parasite culture for *Leishmania* infection were positive by PCR diagnosis and all negative samples by PCR diagnosis were negative by other methods.

Despite its high sensitivity and specificity, PCR diagnosis may have limitations in VL diagnosis. PCR diagnosis alone cannot differentiate between asymptomatic and acute infections of VL (Deborggraeve et al. 2008), thus this method may be used only for the confirmation of suspected cases of acute VL. Currently, asymptotic VL patients in endemic regions are not treated with (Kennedy 1984) drugs because the available drugs for VL are highly toxic and their unnecessary use may stimulate the emergence and spread of drug-resistant parasite strains. However, it should be noted that PCR diagnosis of *Leishmania* DNA in asymptomatic VL patients is beneficial for epidemiological studies.

Table 1 Comparison of PCR amplification, microscopical examination, and parasite culture to diagnose visceral leishmaniasis

	Total	Microscopy		Culture	
		(+)	(−)	(+)	(−)
PCR diagnosis (+)	79 (68.7%)	65	14	20	59
PCR diagnosis (−)	36 (31.3%)	0	36	0	36
Total	115	65 (56.5%)	50 (43.5%)	20 (21.0%)	95 (79.0%)

Acknowledgement We thank Richard Culleton for proofreading the manuscript. KP is a recipient of a Ph.D. scholarship from the Ministry of Education, Culture, Sports, Science and Technology (MEXT) of Japan. This study was supported in part by Grants-in-Aid from MEXT, the Global COE Program at Nagasaki University (to KH and OK), and the National Bio-Resource Project (NBRP) of MEXT, Japan (to KH).

References

Aransay AM, Scoulica E, Tselentis Y (2000) Detection and identification of *Leishmania* DNA within naturally infected sand flies by seminested PCR on minicircle kinetoplastic DNA. Appl Environ Microbiol 66:1933–1938

Sundar S, Mondal D, Rijal S et al (2008) Implementation research to support the initiative on the elimination of kala azar from Bangladesh, India and Nepal—the challenges for diagnosis and treatment. Trop Med Int Health 13:2–5

Al-Jawabreh A, Barghuthy F, Schnur LF, Jacobson RL, Schonian G, Abdeen Z (2003) Epidemiology of cutaneous leishmaniasis in the endemic area of Jericho, Palestine. East Mediterr Health J 9:805–815

Herwaldt BL (1999) Leishmaniasis. Lancet 354:1191–1199

Sundar S (2003) Diagnosis of kala-azar—an important stride. J Assoc Physicians India 51:753–755

da Silva LJ (2005) Vianna and the discovery of *Leishmania braziliensis*: the role of Brazilian parasitologists in the identification of Bauru's ulcer as American leishmaniasis. Parassitologia 47:335–341

Chappuis F, Sundar S, Hailu A et al (2007) Visceral leishmaniasis: what are the needs for diagnosis, treatment and control? Nat Rev Microbiol 5:873–882

Marfurt J, Nasereddin A, Niederwieser I, Jaffe CL, Beck HP, Felger I (2003) Identification and differentiation of *Leishmania* species in clinical samples by PCR amplification of the miniexon sequence and subsequent restriction fragment length polymorphism analysis. J Clin Microbiol 41:3147–3153

Bensoussan E, Nasereddin A, Jonas F, Schnur LF, Jaffe CL (2006) Comparison of PCR assays for diagnosis of cutaneous leishmaniasis. J Clin Microbiol 44:1435–1439

Schallig HD, Oskam L (2002) Molecular biological applications in the diagnosis and control of leishmaniasis and parasite identification. Trop Med Int Health 7:641–651

Reithinger R, Dujardin JC (2007) Molecular diagnosis of leishmaniasis: current status and future applications. J Clin Microbiol 45:21–25

Brustoloni YM, Lima RB, da Cunha RV et al (2007) Sensitivity and specificity of polymerase chain reaction in Giemsa-stained slides for diagnosis of visceral leishmaniasis in children. Mem Inst Oswaldo Cruz 102:497–500

Li J, Wirtz RA, McCutchan TF (1997) Analysis of malaria parasite RNA from decade-old Giemsa-stained blood smears and dried mosquitoes. Am J Trop Med Hyg 57:727–731

Motazedian H, Karamian M, Noyes HA, Ardehali S (2002) DNA extraction and amplification of *Leishmania* from archived, Giemsa-stained slides, for the diagnosis of cutaneous leishmaniasis by PCR. Ann Trop Med Parasitol 96:31–34

Amar C, Pedraza-Diaz S, McLauchlin J (2001) Extraction and genotyping of *Cryptosporidium parvum* DNA from fecal smears on glass slides stained conventionally for direct microscope examination. J Clin Microbiol 39:401–403

Pandey BD, Pandey K, Kaneko O, Yanagi T, Hirayama K (2009) Relapse of visceral leishmaniasis after miltefosine treatment in a Nepalese patient. Am J Trop Med Hyg 80:580–582

Akkafa F, Dilmec F, Alpua Z (2008) Identification of *Leishmania* parasites in clinical samples obtained from cutaneous leishmaniasis patients using PCR-RFLP technique in endemic region, Sanliurfa province, in Turkey. Parasitol Res 103:583–586

Smyth AJ, Ghosh A, Hassan MQ et al (1992) Rapid and sensitive detection of *Leishmania* kinetoplast DNA from spleen and blood samples of kala-azar patients. Parasitology 105(Pt 2):183–192

Salotra P, Sreenivas G, Pogue GP et al (2001) Development of a species-specific PCR assay for detection of *Leishmania donovani* in clinical samples from patients with kala-azar and post-kala-azar dermal leishmaniasis. J Clin Microbiol 39:849–854

Pandey K, Pant S, Kanbara H et al (2008) Molecular detection of *Leishmania* parasites from whole bodies of sandflies collected in Nepal. Parasitol Res 103:293–297

Deborggraeve S, Laurent T, Espinosa D et al (2008) A simplified and standardized polymerase chain reaction format for the diagnosis of leishmaniasis. J Infect Dis 198:1565–1572

Kennedy WP (1984) Novel identification of differences in the kinetoplast DNA of *Leishmania* isolates by recombinant DNA techniques and in situ hybridisation. Mol Biochem Parasitol 12:313–325

Selective accumulation of rhodacyanine in plasmodial mitochondria is related to the growth inhibition of malaria parasites†

Daiki Morisaki,[a] Hye-Sook Kim,[b] Hiroshi Inoue,[a] Hiroki Terauchi,[a] Shusuke Kuge,[a] Akira Naganuma,[a] Yusuke Wataya,[b] Hidetoshi Tokuyama,[a] Masataka Ihara*[ac] and Kiyosei Takasu*[ad]

Received 25th January 2010, Accepted 12th February 2010
DOI: 10.1039/c0sc00125b

Fluorescent rhodacyanines, which display antimalarial activity *in vitro* and *in vivo*, stain plasmodial parasites at the erythrocytic stage. A good correlation between the antimalarial activity and the accumulation of the dyes is observed. A fused-rhodacyanine, which displays a strong fluorescent property itself, was designed as a new probe for plasmodial parasites. It appears to be specifically localized in the parasitic mitochondria.

Introduction

Malaria, which is caused by the infection of *Plasmodium* spp., is one of the most serious tropical diseases. The gravest problem is that the parasites rapidly develop resistance to antimalarial drugs.[1] Particularly, the efficacy of clinically available antimalarials, such as chloroquine (CQ), primaquine, and pyrimethamine, is dramatically decreasing. The development of new antimalarials with novel molecular skeletons and displaying different mechanisms of action against plasmodial parasites to existing drugs is required.[2,3] Recently, we reported that rhodacyanines **1**[4] (Fig. 1), which are structurally unrelated to those compounds commonly used as chemotherapeutics for malaria treatment, show a strong *in vitro* antimalarial activity against *P. falciparum*.[5] Further studies have revealed that they are highly active against chloroquine-resistant strains and that several of them display good *in vivo* efficacy (*P. berghei* mouse models).[6] It is noteworthy that some of the *in vivo* active compounds showed no significant acute toxicity. However, no information on the biological mode of action of antimalarial rhodacyanines has been reported. We describe herein the intracellular behavior of rhodacyanines in the malaria-infected erythrocytes. Furthermore, we report on the good correlation between the antimalarial activity of the rhodacyanines and their accumulation effect in the parasitic mitochondrion.

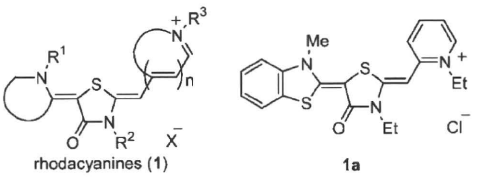

Fig. 1 Rhodacyanines: general structure (left) and representative compound **1a** (right).

Results and discussion

At the outset of our study, the intracellular distribution of **1a**[4] (EC_{50} = 21 nM against *P. falciparum* K1 strain, selective index = >5000 *in vitro*) was examined. Rhodacyanine **1a** itself shows weak fluorescence in response to irradiation with visible light (λ_{ex} = 495 nm, λ_{em} = 516 nm, $\Phi = 2.1 \times 10^{-4}$ in MeOH). Upon the addition of **1a** (final concentration: 5×10^{-6} M) onto cultured human erythrocytes infected with *P. falciparum* and after stirring for 2 h, the cells were fixed as a thin-layered smear on a glass plate and stained using the Diff-Quik® method. In the bright-field image, mature parasites in malaria-infected erythrocytes could be recognized by the optically dense, and brown-black staining of hemozoin in their digestive vacuoles (Fig. 2a). In contrast, fluorescent microscopic observation (through an FITC filter) reveals that **1a**, which is visualized as a red spot, is selectively accumulated in malaria parasites (Fig. 2b). Non-infected host erythrocytes are not stained by **1a**. Additionally, we noted that the selective accumulation can be clearly observed in the living cells (unfixed erythrocytes on the glass plate). Essentially, the accumulation is irreversible; the fluorescent localization is maintained after the treatment with **1a** in infected

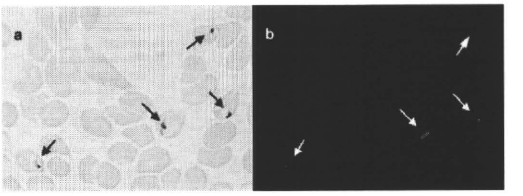

Fig. 2 Microscopic images of the intracellular distribution of **1a** in *P. falciparum*-infected erythrocytes. (a) Bright-field image; parasitic hemozoins (black arrows). (b) Fluorescent image through an FITC filter; **1a** (white arrows).

[a]*Graduate School of Pharmaceutical Sciences, Tohoku University, Aobayama, Sendai 980-8578, Japan*
[b]*Faculty of Pharmaceutical Sciences, Okayama University, Tsushima, Okayama 700-8530, Japan*
[c]*Faculty of Pharmaceutical Sciences, Hoshi University, 2-4-41 Ebara, Tokyo 142-8501, Japan. E-mail: m-ihara@hoshi.ac.jp*
[d]*Graduate School of Pharmaceutical Sciences, Kyoto University, Yoshida, Sakyo-ku, Kyoto 505-8501, Japan. E-mail: kay-t@pharm.kyoto-u.ac.jp; Fax: +81-75-753-4610; Tel: +81-75-753-4610*

† Electronic supplementary information (ESI) available: Color graphics of the accumulation study and characterization data for all new compounds. See DOI: 10.1039/c0sc00125b/

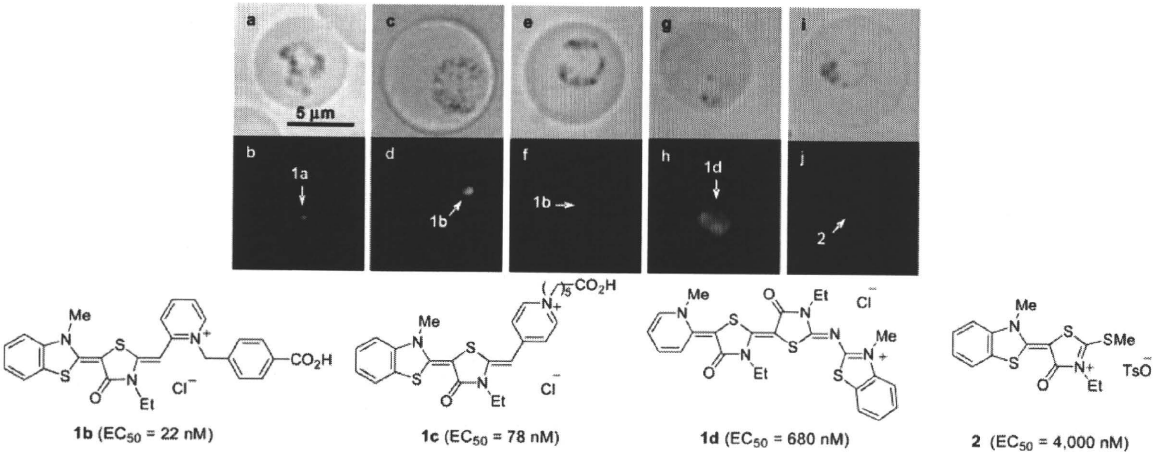

Fig. 3 Accumulation of **1a** (a, b), **1b** (c, d), **1c** (e, f), **1d** (g, h) and **2** (i, j). The final concentration of the rhodacyanines was 5.0×10^{-6} M. Bright-field images (a, c, e, g, i) and fluorescent images through an FITC filter (b, d, f, h, j).

erythrocytes, after washing with PBS (phosphate buffered saline) several times.

The fluorescence distribution of several rhodacyanines and their analogues in the malaria-infected erythrocytes was examined using *P. berghei*. In accordance with the results found for *P. falciparum*, **1a** selectively localizes in the same specific subcellular sites (organelles) of the parasites (Fig. 3a, b).[7] Rhodacyanines displaying strong antimalarial activity, such as **1b** (EC_{50} = 22 nM against *P. falciparum*) also exhibited specific localization. Their fluorescence can be observed as sharp spots (Fig. 3c, d). In contrast, less active compounds like **1d** (EC_{50} = 680 nM) do not show specific concentration into an organelle and instead leach away into the parasitic cytoplasm (Fig. 3g, h), although they still remain in the plasmodial cells (no fluorescence was observed in the erythrocyte cytoplasm). Compound **1c** (EC_{50} = 78 nM against *P. falciparum*) with an intermediate activity shows less specific localization (Fig. 3e, f) compared with **1a** and **1b**. No specific accumulation was observed for much less active compounds like **2** (EC_{50} = 4000 nM; Fig. 3i, j). These observations indicate that there is a good correlation between antimalarial activity and specific accumulation.

Next, we attempted to determine the plasmodial subcellular sites into which the rhodacyanines were selectively accumulated. A multiple-stain experiment with **1a**, DAPI (4′,6-diamino-2-phenylindole; selective staining agent for nuclei) and Diff-Quik® showed that **1a** accumulated in all of the parasitic organelles, except for the nucleus and food vacuoles. However, further investigation could not be carried out owing to the weak fluorescence and/or staining abilities of **1a**.

In order to shed light on the more detailed mechanism, stronger fluorescent probe candidates should be synthesized. We envisaged that fixation of flexible bonds to rhodacyanines would give compounds of improved fluorescent ability due to suppression of energy loss from the excited state to the ground state by vibrational transitions. In this regard, we designed four classes of rhodacyanines **3–6**, which have a fused ring skeleton. The synthetic route to a series of rhodacyanines is shown in Scheme 1.[8] Preparation of **3** started from cyclization of alcohol **7**, followed by condensation with **9** and successive ion exchange. Rhodacyanine **4**, which possesses a pyrrolothiazolinone skeleton as a central core, was synthesized through a 7 step sequence synthesis from **7**. Rhodacyanine **5**, in which rhodanine and pyridine rings are interlocked by an ethylene tether, were synthesized from **14** in 7 steps. Compound **6** was synthesized from ethyl 2-methylnicotinate (**18**). Reaction of 3-aminomethyl-2-methylpyridine (**19**), which was prepared from **18** in three steps, yields rhodanine **20** on treatment with carbon disulfide and methyl bromoacetate in the presence of triethylamine. Then **20** was coupled with methylthiobenzothiazolium salt (**12**) to give **21** in a 69% yield (2 step yield, from **19**). *N*-Methylation of **21** with methyl iodide followed by treatment with methyl triflate in the presence of triethylamine and an ion exchange process afforded fused-rhodacyanine **6** in 42% yield (3 steps).

The antimalarial activity and fluorescent properties of fused-rhodacyanines **3–6** are summarized in Table 1. *In vitro* antimalarial activities (EC_{50}) of **3–6** were shown to be comparable to that of the original rhodacyanine **1a**. Their selective toxicities were excellent as well. As expected, the fluorescence intensities of the new probes are improved over that of **1a**. Especially, compounds **5** and **6** show a 70-fold increase in fluorescence intensity compared to **1a**, and a significant red shift of the fluorescent emission was observed (excitation: λ_{ex} = 495 nm).

With the probes **3–6** in hand, their fluorescent accumulation effects were examined using the *P. berghei* strain. The results are shown in Fig. 4. It is noteworthy that the fluorescence localization of **6** into parasitic organelles can be clearly detected, even upon treatment with a 100-fold less amount of **6** (final concentration; 5×10^{-8} M) compared to the original rhodacyanine **1a**. Double stain experiments of the *P. berghei*-infected erythrocytes co-incubated with **6** and a selective fluorescent marker of subcellular organelle, were performed. As markers of nuclei and mitochondria, DAPI and MitoTracker Red CMXRos® were used, respectively. Microscopic images are shown in Fig. 5 and 6. The studies indicated that rhodacyanine **6** and DAPI were selectively accumulated in different organelles, respectively

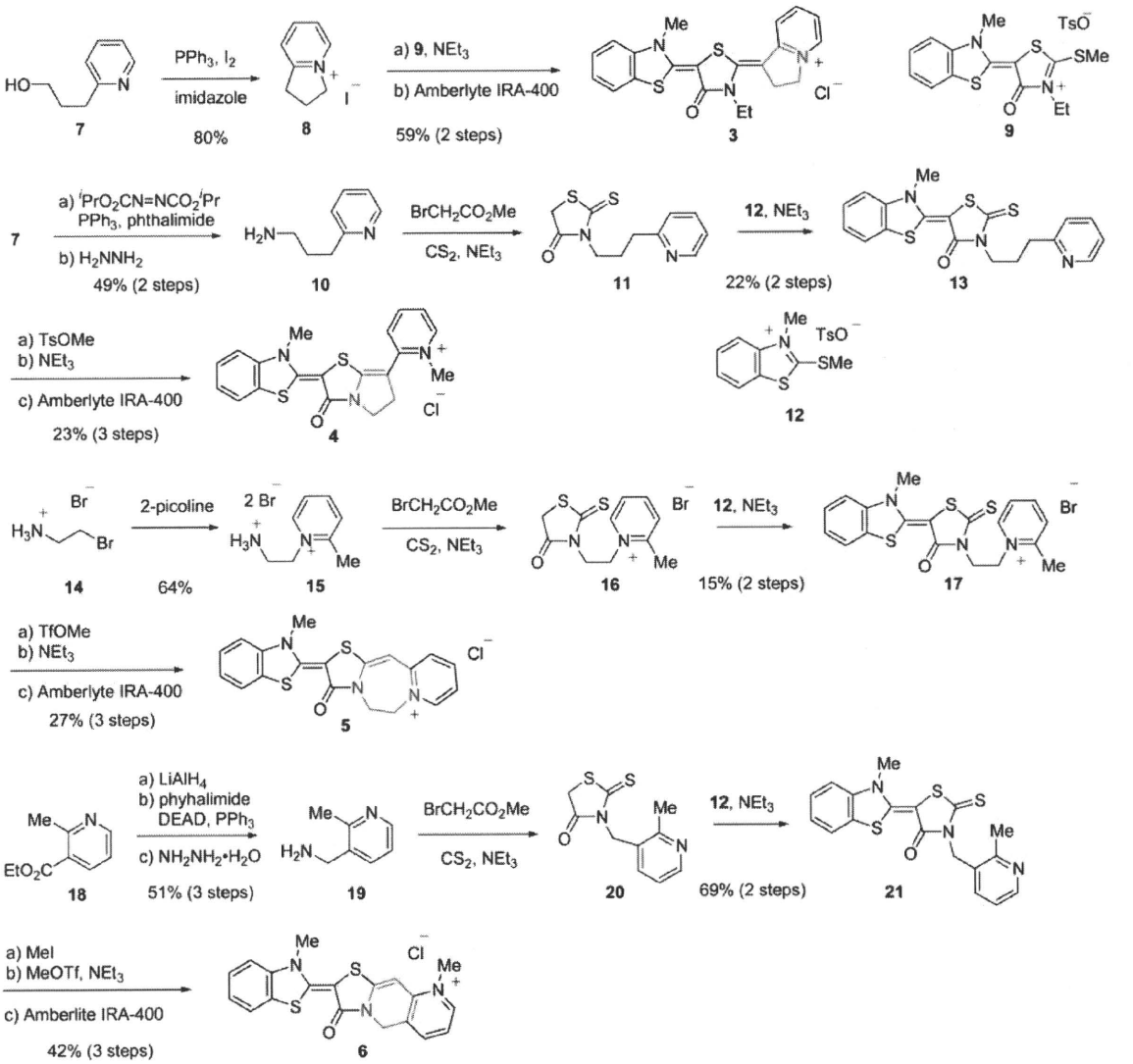

Scheme 1 Synthesis of fused-rhodacyanines **3–6**.

Table 1 *In vitro* antimalarial activity and fluorescent properties of tested compounds

Probe	EC_{50}/nM[a]	Selectivity[b]	λ_{em}/nm[c]	Φ_F[d]
1a	21	>5000	516	2.1×10^{-4}
3	46	3500	548	4.7×10^{-4}
4	64	2300	516	2.9×10^{-3}
5	46	>5000	576	1.4×10^{-2}
6	65	>5000	563	1.4×10^{-2}

[a] *In vitro* antiplasmodial activity against *P. falciparum* K1. [b] Selective toxicity, EC_{50} value for L-6/EC_{50} for *P. falciparum*. Cytotoxicity was evaluated using rat skeletal myoblast L-6 cells representing a model of a host. [c] Maximum with highest wavelength of emission spectra (excitation: λ_{ex} = 495 nm) in MeOH (1.0×10^{-6} M) at 20 °C. [d] Determined relative to fluorescein.

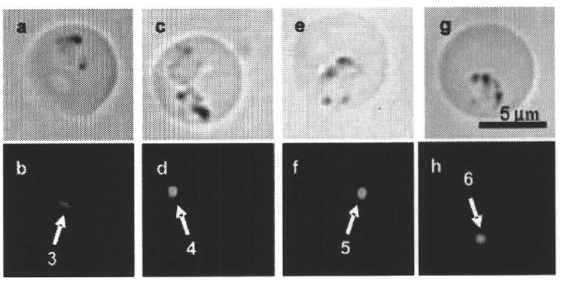

Fig. 4 Accumulation of fused rhodacyanines **3** (a, b), **4** (c, d), **5** (e, f) and **6** (g, h). Their final concentrations were 5.0×10^{-6} M (**3**, **4**), 1.0×10^{-6} M (**5**) and 5.0×10^{-8} M (**6**). Bright-field images (a, c, e, g) and fluorescent images through an FITC filter (b, d, f, h).

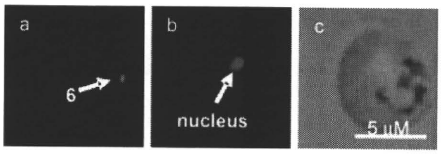

Fig. 5 Fluorescent microscopic images of the intracellular distribution of **6** and DAPI in *P. berghei*-infected erythrocytes, (a) through an FITC filter; **6** (green spot); (b) though a DAPI filter, parasitic nucleus stained by DAPI; (c) superimposed.

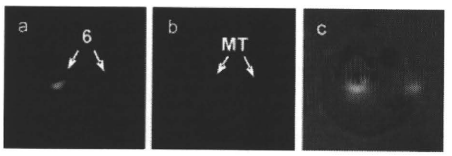

Fig. 6 Fluorescent microscopic images of the intracellular distribution of **6** and CMXRos® in *P. berghei*-infected erythrocytes, (a) through an FITC filter; **6** (green spots); (b) through a Y7 filter, mitochondria (MT) stained by CMXRos® (red spots); (c) superimposed.

(Fig. 5). In contrast, fluorescence localization of **6** is clearly consistent with that of CMXRos (Fig. 6). Thus, we concluded that rhodacyanines selectively accumulate in the plasmodial mitochondria. Fused-rhodacyanine **6** could be used as a visible diagnostic probe for plasmodial mitochondria.[9]

The selective uptake of rhodacyanines in mitochondria is consistent with the DLC (π-delocalized lipophilic cation) hypothesis,[10] which is our starting point for the drug design. The conceptual term DLC was originally proposed by Chen *et al.* in their anticancer research work. It has subsequently been reported that several DLC compounds exhibit selective antitumor activity due to their selective accumulation in the mitochondria of carcinoma cells. This accumulation depends on the mitochondrial membrane potential (negative inside). Our results in this study suggest the DLC hypothesis would also be applicable to antimalarial drug design.[11] It is noteworthy that rhodacyanines are found to display strong antileishmanial activity against *Leishmania* spp.,[12] which are related parasitic protozoa to *Plasmodium* spp. The uptake of rhodacyanines in mitochondria might be a key role in the inhibition of related protozoal diseases.

Conclusions

In summary, we have found that antimalarial rhodacyanines selectively accumulate in erythrocytic plasmodial mitochondria. Furthermore, there is good correlation between their accumulation and antimalarial activity. Thus, the accumulation effect will have a dominant influence on the inhibition of plasmodial growth. It is noteworthy that the newly synthesized rhodacyanine **6** could be applied as a probe for plasmodial parasites as well as their mitochondria since it displays strong fluorescent properties and almost no cytotoxicity. Further studies are undergoing to understand the biological mechanism of action of rhodacyanines in detail.

Acknowledgements

We thank Mr Marcel Kaiser and Prof. Reto Brun for the determination of the EC_{50} values of the synthetic compounds against *P. falciparum* K1. This work was financially supported by Grants-in-Aid from the Intelligent Cosmos Foundation and Japan Science and Technology Agency (JST).

Notes and references

1 (*a*) W. Peters, *Br. Med. Bull.*, 1982, **38**, 187; (*b*) W. H. Wernsdorfer and D. Payne, *Pharmacol. Ther.*, 1991, **50**, 95.
2 P. J. Rosenthal and L. H. Miller, in *Antimalarial Chemotherapy*, ed. P. J. Rosenthal, Humana Press, Totowa, 2001, pp. 3–15.
3 (*a*) M.-L. Go, *Med. Res. Rev.*, 2003, **23**, 456; (*b*) R. G. Ridley, *Nature*, 2002, **415**, 686; (*c*) A. M. Thayer, *Chem. Eng. News*, 2005, **83**(43), 69.
4 M. Kawakami, K. Koya, T. Ukai, N. Tatsuta, A. Ikegawa, K. Ogawa, T. Shishido and L. B. Chen, *J. Med. Chem.*, 1998, **41**, 130.
5 K. Takasu, H. Inoue, H.-S. Kim, M. Suzuki, T. Shishido, Y. Wataya and M. Ihara, *J. Med. Chem.*, 2002, **45**, 995.
6 (*a*) K. Takasu, K. Pudhom, M. Kaiser, R. Brun and M. Ihara, *J. Med. Chem.*, 2006, **49**, 4795; (*b*) K. Pudhom, K. Kasai, H. Terauchi, H. Inoue, M. Kaiser, R. Brun, M. Ihara and K. Takasu, *Bioorg. Med. Chem.*, 2006, **14**, 8550; (*c*) K. Pudhom, J.-F. Ge, C. Arai, M. Yang, M. Kaiser, S. Wittlin, R. Brun, I. Itoh and M. Ihara, *Heterocycles*, 2009, **77**, 207.
7 After verifying similar accumulation effects, we mainly used rodent malaria, *P. berghei*, instead of human malaria, *P. falciparum*, for safety reasons.
8 Syntheses of fused-rhodacyanines **3–5** have been reported in a preliminary communication: K. Takasu, D. Morisaki, M. Kaiser, R. Brun and M. Ihara, *Heterocycles*, 2005, **66**, 161.
9 Although several low-molecular weight compounds have been reported to be visible diagnostic agents for plasmodial parasites, almost all of those stain the parasitic nucleus or cytoplasm. To the best of our knowledge, it has been reported that parasitic mitochondria can be stained only by rhodamine 123, see: (*a*) K. Tanabe, *J. Protozool.*, 1983, **30**, 707; (*b*) A. A. Divo, T. G. Geary, J. B. Jensen and H. Ginsburg, *J. Protozool.*, 1985, **32**, 442.
10 L. B. Chen, *Annu. Rev. Cell Biol.*, 1988, **4**, 155.
11 K. Takasu, T. Shimogama, C. Saiin, H.-S. Kim, Y. Wataya, R. Brun and M. Ihara, *Chem. Pharm. Bull.*, 2005, **53**, 653.
12 (*a*) K. Takasu, H. Terauchi, H. Inoue, M. Takahashi, S. Sekita and M. Ihara, *Heterocycles*, 2004, **54**, 215; (*b*) M. Yang, C. Arai, A. Baker Md, J. Lu, J.-F. Ge, K. Pudhom, K. Takasu, K. Kasai, M. Kaiser, R. Brun, V. Yardley, I. Itoh and M. Ihara, *J. Med. Chem.*, 2010, **53**, 368.

HETEROCYCLES, Vol. 81, No. 5, 2010, pp. 1193 - 1229. © The Japan Institute of Heterocyclic Chemistry
Received, 19th January, 2010, Accepted, 1st March, 2010, Published online, 2nd March, 2010
DOI: 10.3987/COM-10-11912

GERANYL DERIVATIVES OF ISOQUINOLINE ALKALOIDS SHOW INCREASED BIOLOGICAL ACTIVITIES

Yumi Nishiyama,[a] Kinuko Iwasa,[*,a] Suguru Okada,[a] Sousuke Takeuchi,[a] Masataka Moriyasu,[a] Miyoko Kamigauchi,[a] Junko Koyama,[a] Atsuko Takeuchi,[a] Harukuni Tokuda,[b] Hye-Sook Kim,[c] Yusuke Wataya,[c] Kazuyoshi Takeda,[d] Yi-Nan Liu,[e] Pei-Chi Wu,[e] Kenneth F. Bastow,[e] Toshiyuki Akiyama,[e] and Kuo-Hsiung Lee[e]

[a]Kobe Pharmaceutical University, 4-19-1 Motoyamakita, Higashinada-ku, Kobe-shi 658-8558, Japan, [b]Department of Biochemistry and Molecular Biology, Kyoto Prefectural University of Medicine, Kawaramachi-dori, Kamigyo-ku, Kyoto 602-0841, Japan, [c]Faculty of Pharmaceutical Science, Okayama University, Tsushima, Okayama 700, Japan, [d]Yokohama College of Pharmacy, 601 Matanocyo, Hodogayaku, Yokohama-shi 245-0066 Japan, [e]Natural Products Research Laboratories, Eshelman School of Pharmacy, University of North Carolina, Chapel Hill, NC 27599-7360, USA

Abstract – Three types of isoquinoline alkaloids were tested for antimicrobial, cytotoxic, anti-malarial, anti-oxidant, and anti-HIV activities, as well as inhibitory activity against Epstein-Barr virus early antigen (EBV-EA) activation induced by 12-*O*-tetradecanoylphorbol-13-acetate (TPA) in Raji cells. *N*- or *O*-Geranylation contributed to increased potency in four types of activities except anti-HIV and anti-oxidant. Some types of alkaloids may be useful as lead compounds for developing potential chemotherapeutic agents. *N,N*-Geranylated salsolinol was significantly active in three different assays, antimicrobial, cytotoxic, and EBV-EA, and may be a most useful compound.

INTRODUCTION

A number of aromatic prenyltransferases, responsible for prenyl group attachment, have only recently been isolated and characterized.[1-4] Aromatic prenyltransferases catalyze the transfer of a C_5

(dimethylallyl), C_{10} (geranyl) or C_{15} (farnesyl) prenyl group derived from the corresponding isoprenyl diphosphate metabolites onto a variety of electron-rich aromatic acceptors. Prenyl groups appear in a wide variety of bioactive natural products of microbial and plant origin, including amino acids, stilbenes, alkaloids, polyketides and phenylpropanoids such as flavonoids, creating natural product hybrids with altered or enhanced bioactivities. For example, prenylated indole alkaloids containing both aromatic and isoprenoid moieties, are widely distributed in terrestrial and marine organisms.[5] Prenylation appears in many cases to provide a higher level of bioactivity compared to the nonprenylated precursors and sometimes to cause biological activities distinct from those of the parent compounds.[6,7] Thus, prenylated compounds represent a new frontier for the development of novel drugs, in particular, anti-microbial, anti-oxidant, anti-inflammatory, anti-viral, and anti-cancer agents. We have previously tested the antimicrobial, antimalarial, cytotoxic, anti-HIV, and anti-oxidant activities and inhibitory effects on EBV-EA induction of isoquinoline alkaloids.[8,9] Some of the tested isoquinolines showed significant activities in these assays. It was expected that addition of the prenyl group to the isoquinoline alkaloids [simple isoquinolines, 1-benzylisoquinolines, and protoberberines] would increase their potency compared with that of the parent compounds in some assays. In this paper, we describe the synthesis of *N*- and *N*,*N*-geranyl, and *O*- and *O*,*O*-geranyl derivatives of isoquinoline alkaloids and compare their activities with those of non-prenylated compounds in five assays: antimicrobial activity, antimalarial activity, cytotoxicity evaluation,[10] inhibitory effects on EBV-EA induction,[11] free radical scavenging activity, and anti-HIV activity.[12]

RESULTS AND DISCUSSIONS

Chemistry. Geranylation of (±)-salsolinol (**1**)[8] with geranyl bromide and sodium hydride in *N*,*N*-dimethylformamide has been previously described to give the *N*- and *N*,*N*-geranyl derivatives (**2**, **3**).[13] (±)-*N*-Methylsalsolinol (**4**) and quaternary (±)-*N*,*N*-dimethylsalsolinol (**5**) has been prepared from **(±)-carnegine.**[13] Geranylation of **5** by the same methods gave the *O*- and *O*,*O*-geranyl derivatives (**6**-**8**) (Scheme 1). Geranylation of (±)-tetrahydropapaveroline (**9**)[9] gave the *N*- and *N*,*N*-geranyl derivatives (**10** and **11**), and (±)-*N*-methylpapaveroline (**12**) produced the *O*,*O*-geranyl derivative (**13**) (Scheme 2). Geranylation of (±)-2,3,9,10-tetrademethyltetrahydropalmatine (**14**)[9] afforded the *N*-geranyl derivatives (**15** and **16**) and (±)-2,3,10,11-tetrademethylpseudotetrahydropalmatine (**17**)[9] gave the *N*-geranyl derivative (**18**) (Scheme 3). Each geranylated compound was purified by preparative HPLC of the reaction mixtures using NH_4OAc (0.05% TFA)-MeOH (0.05% TFA).

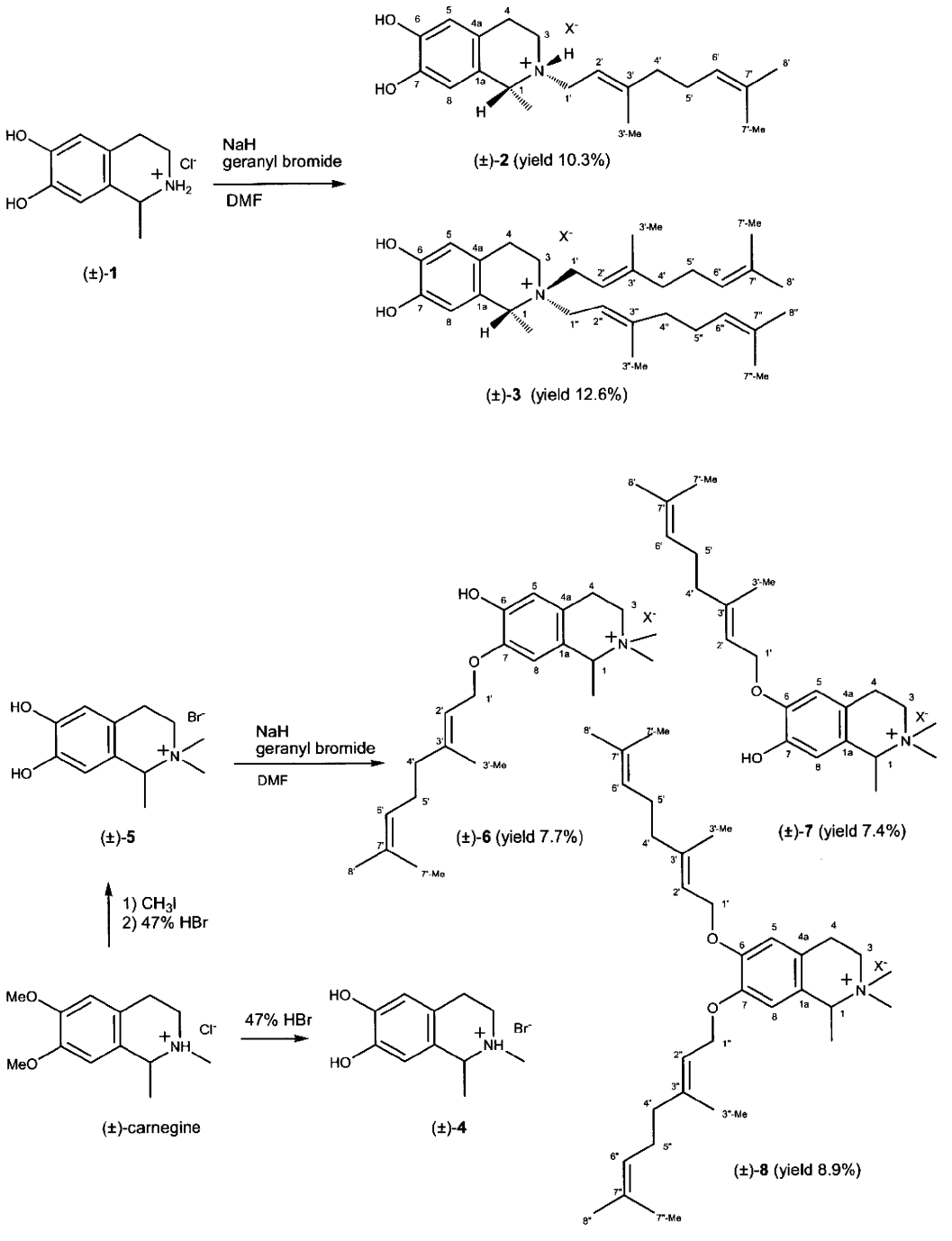

Scheme 1. *N*-geranylation of simple isoquinolines

The HPLC of the reaction mixture in geranylation of salsolinol (**1**) is shown in Figure 1 (I). The peaks a_1 and b_1 were determined to be (±)-*N*-geranylsalsolinol (**2**) and (±)-*N*,*N*-digeranylsalsolinol (**3**), respectively (Scheme 1). Their structures, including the stereostructure, have been previously described:[13] orientation of the C (1)-methyl group is quasi-axial in **2** and **3** and that of the *N*-geranyl group is quasi-equatorial in **2**.

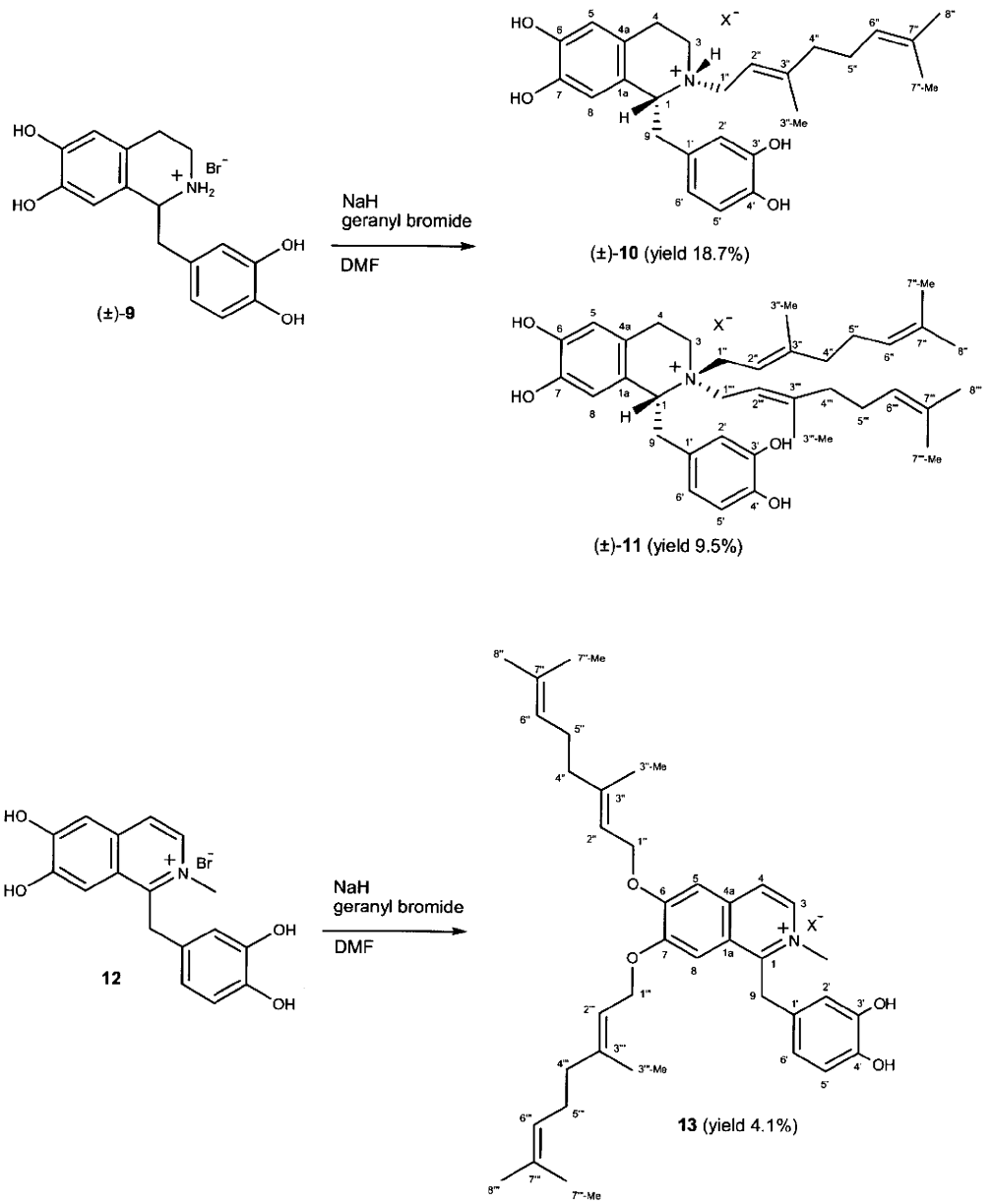

Scheme 2. *N*-geranylation of 1-benzylisoquinolines

These stereostructures were identical with the optimized geometry of **2** and **3** calculated. The optimized geometry and molecular orbital of **2** and **3** were calculated by the DFT (Density Function Theory) method using the Materials Studio DMol3 package of Accelrys Inc.[14,15] (Figure 1) and they may be necessary to clarify the biological activities' mechanisms.

HPLC of the reaction mixture in geranylation of (±)-*N*,*N*-dimethylsalsolinol (**5**) is shown in Figure 1. Compounds **6**-**8**, corresponding to the peaks a_2, b_2, and c_2, respectively, (Figure 1, II) were separated and purified by preparative HPLC. The molecular formula of compound **6** was determined to be $C_{22}H_{34}NO_2$ by analysis of its HRSIMS ($[M]^+$, *m/z* 344.2606), which indicates the presence of one geranyl group.

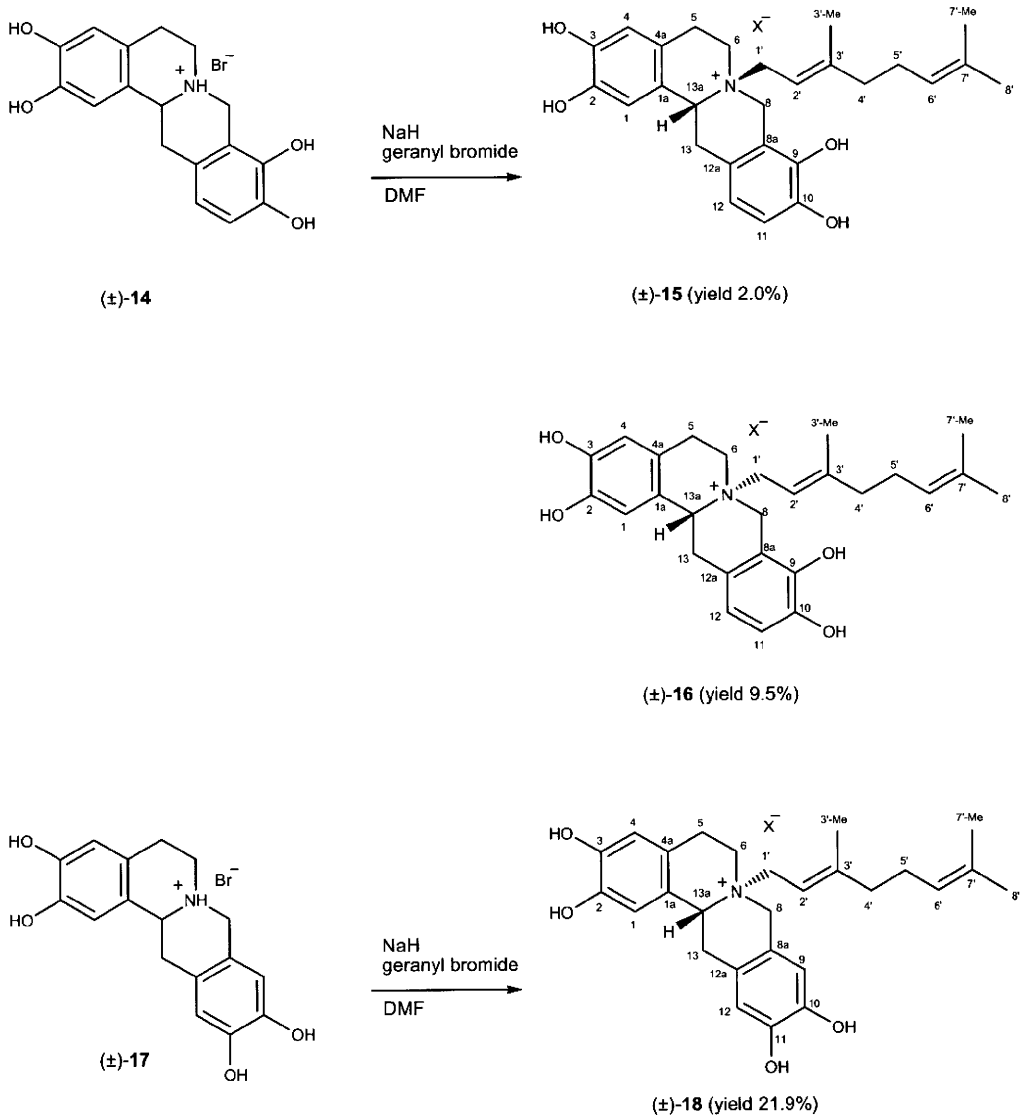

Scheme 3. *N*-geranylation of tetrahydroprotoberberines

The ^{1}H NMR spectrum displays two aromatic proton singlets at δ 6.68 and 6.74, a methine proton at δ 4.57 (q, J = 6.5 Hz), two methylene groups [δ 3.77 (1H), 3.55 (1H), and 3.08 (2H)], two *N*-methyl proton signals [δ 3.17 (3H) and 3.14 (3H)], and a methyl proton signal [δ1.69 (3H, d, J = 6.5 Hz)], characteristic of the isoquinoline moiety, and three methyl proton signals at δ 1.75 (3H, s), 1.65 (3H, s), and 1.59 (3H, s), two olefinic protons at δ 5.48 (1H, t, J = 6.5 Hz) and 5.09 (1H, t, J = 6.5 Hz), and three methylene groups [δ 4.62 (2H, d, J = 6.5), δ 2.12 (2H, m), and δ 2.09 (2H, m)], assignable to the geranyl group. The olefinic protons at δ 5.48 and 5.09 show COSY coupling to the methylene protons at δ 4.62 and 2.12, respectively, which led to the assignment of H-2' (δ 5.48) and H-6' (δ 5.09), respectively. The methylene protons at δ 4.62 and 2.12 were assigned to H_2-1' and H_2-5', respectively.

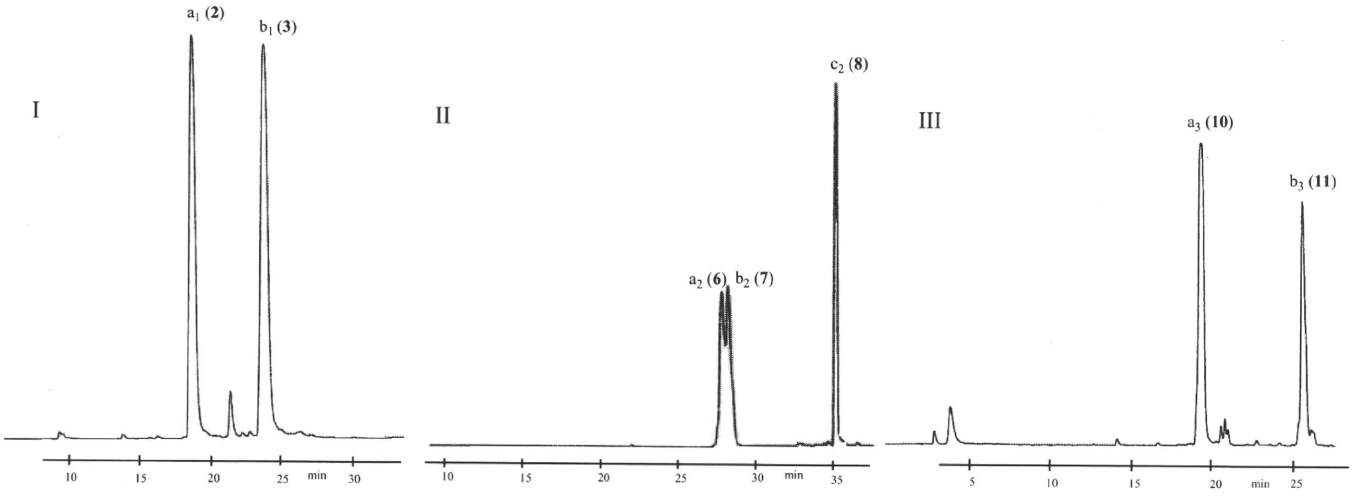

Figure 1. Analytical scale HPLC chromatograms of geranylated products of I: salsolinol (**1**), II: *N*, *N*-dimethylsalsolinol (**5**), and III: tetrahydropapaveroline (**9**) Column: Cosmosil 5C18-ARII (6.0 x 150 mm); Eluent: A:0.1M NH4OAc (0.05% TFA), B:MeOH (0.05% TFA), I and II [A/B: 80/20 (initial) 0/100 (30 min)]; III [A/B: 75/25 (initial) 50/50 (10 min) 0/100 (30 min)]; Flow rate: 1 mL/min; Detector: UV(280 nm)

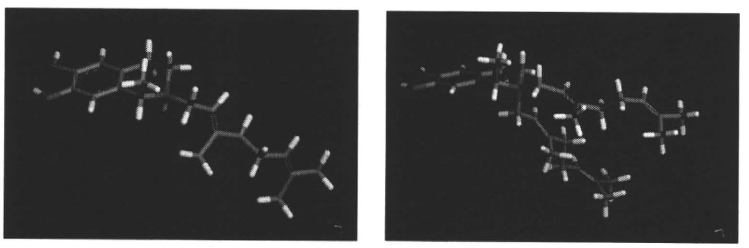

Optimized geometry of *N*-geranylsalsolinol (**2**) E=-986.0139433 Ha (BLYP/DNP)

Optimized geometry of *N*,*N*-digeranylsalsolinol (**3**) E=-1376.8807811 Ha (BLYP/DNP)

The NOE correlations between an aromatic proton at δ 6.74 and a proton at δ 4.57 (H-1) indicated that this aromatic proton was assigned as H-8. The aromatic proton at δ 6.68, which was correlated with the methylene protons at δ 3.08 (H_2-4) was assigned as H-5. NOE correlations were also observed between the aromatic proton at δ 6.74 (H-8) and methylene protons at δ 4.62 (H-1'), indicating that a geranyl group was attached to oxygen at C-7. Based on the above evidence, compound **6** was indicated to be 7-*O*-geranyl-*N*, *N*-dimethylsalsolinol (Scheme 1). Moreover, the ^{13}C NMR spectrum of **6** supports this assignment, with signals corresponding to 22 carbons, including two protonated olefinic carbons (δ 124.90; 120.94), two protonated aromatic carbons (δ 116.01; 113.25), six quaternary carbons (δ 148.79; 147.83; 142.30; 132.63; 124.39; 122.17), five methylene carbons (δ 67.06; 56.86; 40.61; 27.41; 24.30), a methine carbon (δ 69.51), two *N*-methyl carbons (δ 51.50; 50.11) and four methyl carbons (δ 25.84; 18.63; 17.72; 16.69). The carbon signal at δ 147.83 (C-7) displays HMBC correlations with the proton signal at δ 4.62 (H-1'), confirming 7-*O*-geranylation, which was already suggested by the NOE correlation between H-8 and H-1'. On the basis of these data, the structure of **6**

was established to be **(±)-**7-*O*-geranyl-*N*,*N*-dimethylsalsolinol.

The molecular formula of compound **7** was determined to be $C_{22}H_{34}NO_2$ by analysis of its HRSIMS ($[M]^+$, *m/z* 344.2603), which indicated the presence of one geranyl group. The ^{1}H NMR spectrum is almost the same with that of **6**. The NOE correlations between the aromatic proton at δ 6.66 and δ 4.55 (H-1) and the aromatic proton at δ 6.79 and the methylene protons at δ 3.12 (H_2-4) indicate that the aromatic protons at δ 6.66 and 6.79 were assigned to H-8 and H-5, respectively. NOE correlations were also observed between the aromatic proton at δ 6.79 (H-5) and methylene protons at δ 4.63 (H-1'), indicating that a geranyl group is attached to oxygen at C-6. Based on the above evidence, compound **7** was found to be 6-*O*-geranyl-*N*,*N*-dimethylsalsolinol (Scheme 1). Moreover, the ^{13}C NMR spectrum of **7** supports this structure, with signals corresponding to 22 carbons. The carbon signal at δ 148.62 (C-6) display HMBC correlations with the proton signal at δ 4.63 (H-1'), confirming 6-*O*-geranylation, which was suggested by the NOE correlation between H-5 and H-1'. On the basis of these data, the structure of **7** was confirmed to be **(±)-**6-*O*-geranyl-*N*,*N*-dimethylsalsolinol.

The molecular formula of compound **8** was determined to be $C_{32}H_{50}NO_2$ by analysis of its HRSIMS ($[M]^+$, *m/z* 480.3858), which indicated the presence of two geranyl groups. The ^{1}H NMR spectrum displays two aromatic protons as singlets at δ 6.83 and 6.79, a methine proton at δ 4.54 (q, J = 6.5 Hz), two methylene groups [δ 3.79 (1H), 3.57 (1H), and 3.14 (2H)], two *N*-methyl groups [δ 3.17 (3H) and 3.15 (3H)], and a methyl proton signal [δ 1.69 (3H, d, J = 6.5 Hz)], characteristic of an isoquinoline moiety, and six methyl proton signals at δ 1.66 (6H, s), 1.60 (6H, s), 1.736 (3H, s), and 1.742 (3H, s), four olefinic protons at δ 5.48 (2H) and 5.10 (2H), and six methylene groups [δ 4.58 (2H), 4.59 (2H), 2.12 (4H, m), and δ 2.07 (4H)], assignable to two geranyl groups. The aromatic proton at δ6.83 shows NOE correlations with both methylene protons at δ 3.14 (H-4) and 4.58 (or 4.59, H-1'). This aromatic proton was assigned H-5. Therefore, the geranyl group is attached to the oxygen at C-6. The aromatic proton at δ 6.79 displays NOE correlations with protons at δ 4.54 (H-1), 4.59 (or 4.58, H-1''), and 1.69 (1-Me) indicating that this aromatic proton was H-8. This indicated that the other geranyl group is attached to the oxygen at C-7. From these data, the structure of **8** was deduced to be 6, 7-*O*-digeranyl-*N*,*N*-dimethylsalsolinol (Scheme 1). The ^{13}C NMR spectrum of **8** supports this structure.

Assignments of ^{1}H and ^{13}C signals of **6-8** were made by 1D and 2D (^{1}H-^{1}H COSY, NOESY, HSQC, and HMBC) spectroscopic data. The geometry of the disubstituted olefinic bonds (between 2' and 3' or 2'' and 3'') was determined to be *E* on the basis of the NOE correlation between H-2' and H-4'or H-2'' and H-4'', respectively. The NOE correlations between H-1 and both quasi-equatorial and quasi-axial *N*-methyl groups indicate the quasi-equatorial orientation of H-1, that is, quasi-axial orientation of the methyl group at C-1. These stereostructures were identical with the optimized geometry of **6-8**

calculated.

HPLC of the reaction mixture in geranylation (Scheme 2) of (±)-tetrahydropapaveroline (**9**) is shown in Figure 1 (III). The compounds corresponding to the peaks a_3 and b_3 (Figure 1, III) (**10** and **11**) were purified by prep. HPLC of the reaction mixture. The molecular formula of compound **10** (peak a_3) was determined to be $C_{26}H_{34}NO_4$ by analysis of its HRSIMS ($[M + H]^+$, *m/z* 424.2494), which indicates the presence of one geranyl group. The ^1H NMR spectrum displays two aromatic proton singlets at δ 6.65 and 6.18, a methine proton at δ 4.42 (1H, t, J = 6.5 Hz), two methylene groups [δ 3.68 (1H), 3.38 (1H), and 2.97 (2H)] arisen from the isoquinoline moiety, three aromatic protons at δ 6.75 (1H, d, J = 8.5 Hz), 6.50 (1H, brd, J = 8.5 Hz), and 6.58 (1H, brs), methylene protons [δ 3.04 (1H) and 3.14 (1H)] characteristic of a benzyl group, and three methyl proton signals at δ 1.70 (3H, s), 1.64 (3H, s), and 1.57 (3H, s), two olefinic protons at δ 5.26 (1H, m) and 5.12 (1H, m), and three methylene groups [δ 3.83 (1H), δ 3.71 (1H), and δ 2.18 (4H)], assignable to a geranyl group. The NOE correlations between the methylene protons (H-1'') of the geranyl group and both the methine proton (H-1) of the isoquinoline structure and the methylene protons (H-9) of the benzyl group indicate that the geranyl group was attached to nitrogen. Based on the these evidences, compound **10** was established to be (±)-*N*-geranyltetrahydropapaveroline (Scheme 2). The ^{13}C NMR spectrum of **10** supports this structure, with signals corresponding to 24 carbons (two carbons overlap), including two protonated olefinic carbons (δ 124.56; 114.15), five protonated aromatic carbons (δ 121.87; 117.67; 116.76; 116.12; 115.75), nine quaternary carbons (δ 149.65; 147.30; 146.92; 146.04; 145.65; 133.29; 121.93; 121.87x2), six methylene carbons (δ 51.86; 44.80; 40.74x2; 27.14; 22.90), a methine carbon (δ 63.01), and three methyl carbons (δ 25.94; 17.84; 16.80). Assignments of ^1H and ^{13}C signals of **10** were made by 1D and 2D (^1H-^1H COSY, NOESY, HSQC, and HMBC) spectroscopic data. The geometry of the disubstituted olefinic bond (between 2'' and 3'') was determined to be *E* on the basis of the NOE correlation between H-2'' and H-4''. The geranyl group may be a quasi-equatorial orientation, because a methylene proton (H-1'') of the geranyl group displayed NOE correlations with both the methine proton (H-1) of the isoquinoline structure and the methylene protons (H-9) of the benzyl group. Therefore, the benzyl group is considered to be quasi-axial orientation. The upfield shift (+ 3.6 ppm) at C-3 in **10** compared with *N*-methylsalsolinol (**4**) is interpreted as being due to larger steric compression by the quasi-axial benzyl group at C-1 in **10** than that by the quasi-axial methyl group at C-1 in **4**.

The molecular formula of compound **11** (peak b_3) was determined to be $C_{36}H_{50}NO_4$ by analysis of its HRSIMS ($[M]^+$, *m/z* 560.3746), which indicates the presence of two geranyl groups. The ^1H NMR and ^{13}C NMR spectra of **11** display the signals due to the 1-benzyltetrahydroisoquinoline structure and two sets of signals due to two geranyl groups. The protons at δ 3.78 (H-1") and 4.13 (H-1"') show HMBC

correlations with carbons at δ 58.30 (C-1''') and 55.79 (C-1''), respectively. Furthermore, HMBC correlations were observed from protons at δ 3.96 (H-1'') and δ 4.13 (H-1''') to the carbon at δ 52.01 (C-3). The proton at δ 4.20 (H-1''') also shows a correlation with the carbon at δ 70.72 (C-1). It was concluded that both geranyl groups are attached to nitrogen on the basis of these HMBC correlations, as well as by NOE correlations between H-1 (δ 4.42) and H-1'' (δ 3.96), H-3 (δ 3.53) and H-1''' (δ 4.20), and H-3 (δ 3.68) and H-1''' (δ 4.13 and δ 4.20), respectively. Assignments of ^{1}H and ^{13}C signals of **11** were made by 1D and 2D (^{1}H-^{1}H COSY, NOESY, HSQC, and HMBC) spectroscopic data. Based on these evidences, compound **11** was determined to be **(±)-*N*,*N*-digeranyltetrahydropapaveroline** (Scheme 2). The geometries of the disubstituted olefinic bonds (between 2'' and 3'' and between 2''' and 3''') were determined to be *E* on the basis of the NOE correlations between H-2'' and H-4'', and H-2''' and H-4''', respectively. NOE correlations were observed between the proton at δ 4.20 (H-1''') and H_2-3 at δ 3.68 and 3.53 (quasi-axial and quasi-equatorial protons), indicating that C-1''' of the geranyl group is a quasi-equatorial orientation. The quasi-equatorial orientation of the proton at C-1 was suggested by the NOE correlations between the methine proton at δ 4.42 (H-1) and the proton (δ 3.96) of C-1'' of the quasi-axial geranyl group. Therefore, the orientation of the benzyl group is quasi-axial. This was suggested from the fact that the upfield shift (+ 4.1 ppm) at C-3 in **11** compared with *N*, *N*-dimethylsalsolinol (**5**) arises from larger steric compression by the quasi-axial benzyl group at C-1 in **11** than that by the quasi-axial methyl group at C-1 in **5**.

HPLC of the reaction mixture in geranylation (Scheme 2) of *N*-methylpapaveroline (**12**) is shown in Figure 2 (I). Some compounds (peaks a_4, b_4, and d_4) in the reaction mixture changed during prep.

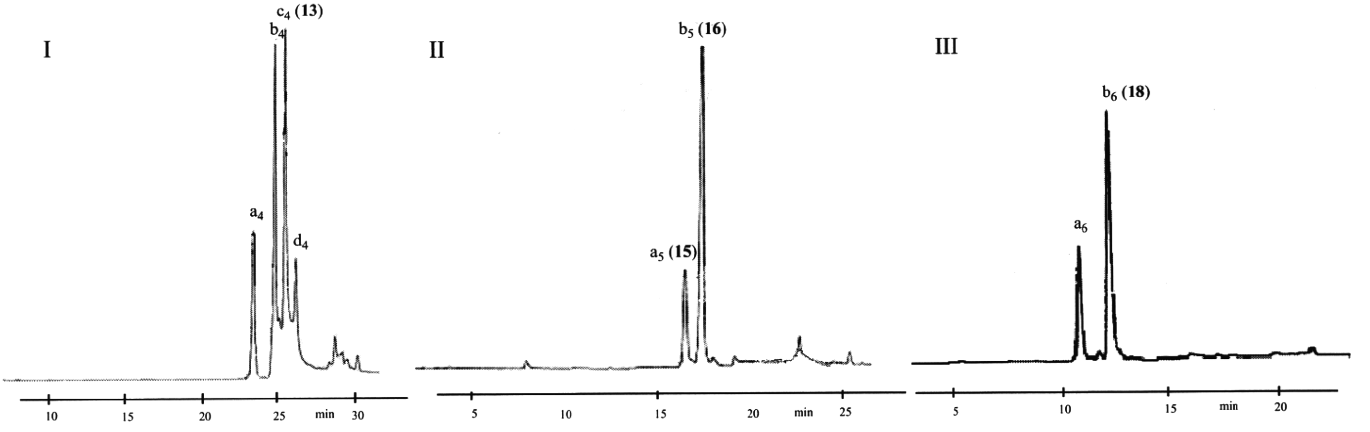

Figure 2. Analytical scale HPLC chromatograms of products obtained by geranylation of I: *N*-methylpapaveroline (**12**), II: 2, 3, 9, 10-tetrademethyltetrahydropalmatine (**14**), and III: 2, 3, 10, 11-tetrademethylpseudotetrahydropalmatine (**17**) Column: Cosmosil $5C_{18}$-ARII (6.0 x 150 mm); Eluent: A:0.1M NH_4OAc (0.05% TFA), B:MeOH (0.05% TFA), I [A/B: 75/25 (initial) 50/50 (10 min) 0/100 (30 min)], II and III [A/B: 80/20 (initial) 0/100 (20 min); Flow rate: 1 mL/min; Detector: UV(280 nm)

HPLC and were not purified. Only peak c_4 was purified by prep. HPLC. The molecular formula of compound **13** (peak c_4) was determined to be $C_{37}H_{48}NO_4$ by analysis of its HRSIMS ($[M]^+$, *m/z* 570.3592), which indicates the presence of two geranyl groups. The ^1H NMR spectrum displays two aromatic protons as doublets at δ 8.32 and 8.08 (J = 7.0 Hz), two aromatic protons as singlets at δ 7.70 and 7.60 originating in the isoquinoline moiety, three aromatic protons at δ 6.71 (1H, d, J = 8.5 Hz), 6.36 (1H, dd, J = 8.5, 1.5 Hz), and 6.49 (1H, d, 1.5 Hz), a methylene proton at δ 4.83 (2H) characteristic of a benzyl group, six methyl proton signals at δ 1.83 (3H, s), 1.70 (3H, s), 1.61 (3H, s), 1.59 (3H, s), 1.58 (3H, s), and 1.55 (3H, s), four olefinic protons at δ 5.58 (1H), 5.39 (1H), 5.09 (1H), and 5.02 (1H), and six methylene groups [δ 4.90 (2H), 4.80 (2H), 2.15 (2H), 2.13 (2H), 2.05 (2H), and 1.98 (2H)], assignable to two geranyl groups. The aromatic proton at δ 7.60 shows NOE correlations with both protons at δ 8.08 (H-4) and 4.90 (H-1''). Thus, the proton at δ 7.60 was assigned to H-5. Therefore, the geranyl group is attached to the oxygen at C-6. The aromatic proton at δ 7.70 displays NOE correlations with protons at δ 4.80 (H-1'''), indicating that this proton is H-8. This indicates that the other geranyl group is attached to the oxygen at C-7. Based on these evidences, compound **13** was identified as *O,O*-digeranylpapaveroline (Scheme 2). Moreover, the ^{13}C NMR spectrum of **13** shows four protonated olefinic carbons (δ 124.91; 124.84; 119.65; 119.32), seven protonated aromatic carbons (δ 136.61; 123.58; 120.39; 117.14; 116.13; 108.15; 108.08), 12 quaternary carbons (δ 158.86; 156.93; 154.18; 147.50; 146.17; 144.48; 143.93; 137.50; 132.81; 132.63; 126.47; 125.62), seven methylene carbons (δ 67.71; 67.33; 40.63; 40.46; 34.96; 27.30; 27.29), one *N*-methyl carbon (δ 46.28), and six methyl carbons (δ 25.91; 25.87; 17.82; 17.81; 16.88; 16.84). The carbon signal at δ 158.86 (C-6) displayed HMBC correlations with the proton signal at δ 4.90 (H-1''), confirming 6-*O*-geranylation, which was also suggested by the NOE correlation between H-5 and H-1''. The carbon signal at δ 154.18 (C-7) displayed HMBC correlations with the proton signal at δ 4.80 (H-1'''), confirming 7-*O*-geranylation, which was corroborated by the NOE correlation between H-8 and H-1'''. Assignments of ^1H and ^{13}C signals of **13** were made by 1D and 2D (^1H-^1H COSY, NOESY, HSQC, and HMBC) spectroscopic data. On the basis of this evidence, the structure of **13** was established to be *O, O*-digeranylpapaveroline (Scheme 2). The geometries of the disubstituted olefinic bonds (between 2'' and 3'' and between 2''' and 3''') were determined to be *E* on the basis of the NOE correlation between H-2'' and H-4'', and between 2''' and 3''', respectively.

HPLC of the reaction mixture in geranylation (Scheme 3) of 2, 3, 9, 10-tetrademethyltetrahydropalmatine (**14**) is shown in Figure 2 (II). The compounds corresponding to peaks a_5 and b_5 (Figure 2, II) (**15** and **16**) were purified by prep. HPLC. The molecular formula of compound **15** (peak a_5) was determined to be $C_{27}H_{34}NO_4$ by analysis of its HRSIMS ($[M]^+$, *m/z* 436.2486), which indicates the presence of one

geranyl group. The ^{1}H NMR spectrum displays two aromatic proton singlets at δ 6.72 and 6.66, two aromatic proton doublets at δ 6.78 (1H, d, J = 8.0 Hz), 6.57 (1H, d, J = 8.0 Hz), methine and methylene protons at δ 4.58 (3H, brs), three methylene groups [δ 3.81 (1H), 3.54 (1H), 3.28 (1H), 3.18 (2H), 3.12 (1H)] arising from the protoberberine moiety and three methyl proton signals at δ 1.65 (3H, s), 1.59 (3H, s), and 1.58 (3H, s), two olefinic protons at δ 5.44 (1H, t, J = 8.0 Hz) and 5.08 (1H, brs), and three methylene groups [δ 4.08 (2H), 2.22 (2H), and 2.20 (2H)], assignable to the geranyl group. The NOE correlations between a methylene proton (δ 4.08, H-1') of the geranyl group and the protons at δ 4.58 (H-8 and/or H-13a) indicate that the geranyl group is attached to nitrogen. Based on these evidences, compound **15** was determined to be *N*-geranyl-2, 3, 9, 10-tetrademethyltetrahydropalmatinium salt. The ^{13}C NMR spectrum of **15** supports this structure, with signals corresponding to 26 (one carbon was overlapped) carbons including four protonated aromatic carbons (δ 119.69; 116.59x2; 114.52), eight quaternary carbons (δ 147.66; 146.25; 144.85; 143.60; 124.76; 121.90; 120.93; 114.80), four methylene carbons (δ 57.06; 51.66; 34.89; 23.75), and a methine carbon (δ 64.34) which arise from the tetrahydroprotoberberine structure, and two protonated olefinic carbons (δ 124.12; 111.74), two quaternary carbons (δ 152.82; 133.47), three methylene carbons (δ 59.93; 41.04; 26.97), three methyl groups (δ 25.78; 17.79; 16.94) assignable to the geranyl group. Assignments of ^{1}H and ^{13}C signals of **15** were made by 1D and 2D (^{1}H-^{1}H COSY, NOESY, HSQC, and HMBC) spectroscopic data. On the basis of these data, the structure of **15** was established to be (±)-*N*-geranyl-2,3,9,10-tetrademethyl-tetrahydropalmatinium salt with the B/C-*cis* form as described later (Scheme 3).

The molecular formula of compound **16** (peak b_5) was determined to be $C_{27}H_{34}NO_4$ by analysis of its HRSIMS ($[M]^+$, *m/z* 436.2484), which indicates the presence of one geranyl group. The ^{1}H NMR spectrum displays two aromatic proton singlets at δ 6.84 and 6.71, two aromatic proton doublets at δ 6.85 and 6.77 (J = 8.2 Hz), a methine proton at δ 5.07 (1H, dd, J = 12.5, 5.0 Hz), and four methylene groups [δ 4.72 (1H, d, J = 15.5 Hz), 4.17 (1H, d, J = 15.5 Hz), 3.89 (1H), 3.83 (1H), 3.69 (1H), 3.26 (1H), 3.20 (1H), and 3.05 (1H)] which arise from the tetrahydroprotoberberine structure, and three methyl proton signals at δ 1.72 (3H, s), 1.66 (3H, s), and 1.33 (3H, s), two olefinic protons at δ 5.44 (1H, dd, J = 9.0, 5.5 Hz) and 5.14 (1H, brs), and three methylene groups [δ 3.86 (1H, m), 3.61 (1H, m), and δ 2.20 (4H, m)], assignable to the geranyl group. The NOE correlation between one of the methylene protons (δ 3.86, H-1') of the geranyl group and one of the methylene protons (δ 4.72, H-8) indicates that the geranyl group is attached to nitrogen. Based on these evidences, compound **16** was postulated to be the isomer of *N*-geranyl-2,3,9,10-tetrademethyltetrahydropalmatininium salt (**15**). Moreover, the ^{13}C NMR spectrum of **16** supports this structure, with signals corresponding to 27 carbons, including four protonated